ACCOUNTS of chemical research

pubs.acs.org/accounts Article

Interplay between Chemical Transformations and Atomic Structure in Nanocrystals and Nanoclusters

Published as part of the Accounts of Chemical Research special issue "Transformative Inorganic Nanocrystals".

Haixiang Han,[†] Yuan Yao,[†] and Richard D. Robinson*

Cite This: *Acc. Chem. Res.* 2021, 54, 509–519 Read Online

ACCESS | Metrics & More | Article Recommendations

CONSPECTUS: Chemically induced transformations are postsynthetic processing reactions applied to first generation (as-synthesized) nanomaterials to modify property-defining factors such as atomic structure, chemical composition, surface chemistry, and/or morphology. Compared with conditions for direct synthesis of colloidal nanocrystals, postsynthetic chemical transformations can be conducted in relatively mild conditions with a more controllable process, which makes them suitable for the precise manipulation of nanomaterials and for trapping metastable phases that are typically inaccessible from the conventional synthetic routes. Each of the chemically induced transformations methods can result in substantial restructuring of the atomic structure, but their transformation pathways can be very different. And the converse is also true: the atomic structure of the parent material plays a large role in the pathway toward and the resulting chemically transformed product. Additionally, the characteristic length of the parent material greatly affects the structure, which affects the outcome of the reaction.

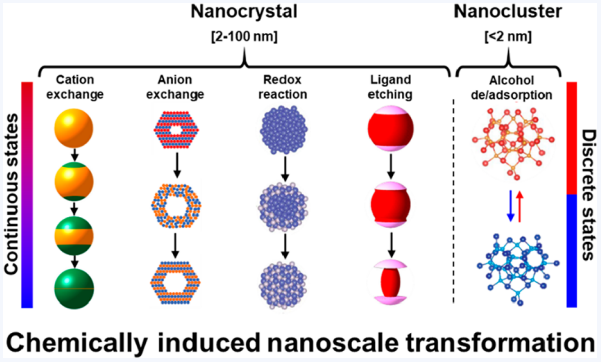

Chemically induced nanoscale transformation

In this Account, we show how the atomic structure and nanoscale size directs the product formation into materials that are inaccessible from analogous chemically transformations in bulk materials. Through examples from the three chemical transformation processes (cation/anion exchange, redox reactions, and ligand exchange and ligand etching), the effect of the atomic structure on chemical transformations is made apparent, and vice versa. For cation exchange, an anisotropic atomic lattice results in a unidirectional exchange boundary. And because the interface can extend through the full crystal, a substantial strain field can form, influencing the phase of the material. In the redox reaction that leads to the nanoscale Kirkendall effect, the atomic structure is the key to inverting the diffusion rates in a diffusion couple to form the hollow cores. And for ligand etching, if one of the materials in a heterostructure has a defected and\or defect-tolerant atomic structure, it can be preferentially etched and its atomic structure can undergo phase transformations while the other composition remains intact. For length scales, we show how the chemically induced transformations greatly differ between bulk, nanocrystal, and nanocluster characteristic sizes. For instance, the structural transformation on relatively large nanocrystals (2−100 nm) can be a continuous process when the activation volume is smaller than the nanocrystal, while for smaller nanoclusters (<2 nm) the transformation kinetics could be swift resulting in only discrete thermodynamic states. Comparing the two nanosystems (nanocrystals to small nanoclusters), we address how their atomic structural differences can direct the divergent transformation phenomena and the corresponding mechanisms. Understanding the nanoscale mechanisms of chemically induced transformations and how they differ from bulk processes is key to unlocking new science and for implementing this processing for functional materials.

KEY REFERENCES

- Ha, D.-H.; Caldwell, A. H.; Ward, M. J.; Honrao, S.; Mathew, K.; Hovden, R.; Koker, M. K. A.; Muller, D. A.; Hennig, R. G.; Robinson, R. D. Solid−Solid Phase Transformations Induced through Cation Exchange and Strain in 2D Heterostructured Copper Sulfide Nanocrystals. *Nano Lett.* **2014**, *14*, 12, 7090−7099.[1] *This study reports how cation exchange on an anisotropic atomic structure results in a dual interface epitaxial heterostructure, whose atomic phase is manipulated by the opposing forces from the cation diffusion and the interfacial strain field.*

Received: October 29, 2020
Published: January 12, 2021

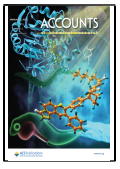

https://dx.doi.org/10.1021/acs.accounts.0c00704
Acc. Chem. Res. 2021, 54, 509−519

- Ha, D.-H.; Moreau, L. M.; Bealing, C. R.; Zhang, H.; Hennig, R. G.; Robinson, R. D. The Structural Evolution and Diffusion During the Chemical Transformation from Cobalt to Cobalt Phosphide Nanoparticles. *J. Mater. Chem.* **2011**, *21*, 31, 11498−11510.[2] *This report highlights the structure-directed diffusion processes that occur during the nanoscale Kirkendall effect, with inward diffusion dominating until the shell material crystallizes and inverts the rates in the diffusion couple, resulting in a hollow core.*
- Nelson, A.; Ha, D.-H.; Robinson, R. D. Selective Etching of Copper Sulfide Nanoparticles and Heterostructures through Sulfur Abstraction: Phase Transformations and Optical Properties. *Chem. Mater.* **2016**, *28*, 23, 8530−8541.[3] *This study reports on the trialkylphosphine-ligand induced selective phase transformations and etching of one component of a heterostructured nanocrystal, governed by the atomic structures.*
- Williamson, C. B.; Nevers, D. R.; Nelson, A.; Hadar, I.; Banin, U.; Hanrath, T.; Robinson, R. D. Chemically Reversible Isomerization of Inorganic Clusters. *Science* **2019**, *363*, 6428, 731−735.[4] This study reports the first instance of reversible isomerization in inorganic materials, where the atomic structures switches discretely between two stable atomic states via a chemically induced, diffusionless transformation.

1. INTRODUCTION

Chemical transformation of nanocrystals and nanoclusters (CTNs) are the reactions that are performed on the first-generation (as-synthesized) nanocolloids that effectively modify their atomic structure, chemical composition, particle size, and morphology.[5,6] The motivations behind CTN research are to understand how and if the mechanisms for these reactions differ at the nanoscale compared to bulk, to expand the scope of existing functional materials,[7] and to explore new metastable phases that are inaccessible from a conventional synthetic approach.[8] CTNs can produce new nanomaterial forms with novel properties that are useful in applications, such as catalysis,[9−12] biosensing,[13,14] optical devices,[15] solar cells,[16] and transistors,[17,18] significantly fostering the development of the materials engineering for device integration.[19] These examples clearly show the power of chemical transformation approach to finely tune the properties of nanomaterials to make them suitable for specific application. For example, through a cation exchange process, a mixed cesium and formamidinium lead triiodide perovskite system achieves great energy conversion efficiency[16] and $CuInSe_2$ colloidal nanocrystals demonstrate good performance as a field effect transistor.[17] CTNs can be realized through several postsynthetic methods such as redox reactions,[20] ion exchange (cation exchange and anion exchange),[21,22] and ligand treatment (ligand exchange and ligand etching),[23,24] all of which are typically conducted in relatively mild conditions (e.g., at room temperature), compared to direct synthesis techniques like hot injection or the heat-up method. Each method can induce different compositional/structural transformations through a variety of pathways typical and atypical of common phase transformations. Likewise, the initial and transitional atomic structure plays a key role in directing the transformation product. The interplay between the chemical transformation and the atomic structure has a complex dependency on a variety of factors including: the size of the parent nanocrystals,[21,25] the phase for the starting and ending nanocrystals,[26,27] preferential tendencies of cation diffusion and crystal growth in multicomponent systems,[28] lattice mismatch, cation diffusion, and surface energy,[29] crystal vacancies,[30] volumetric change between the parent and child unit cell,[31] and extent of the transformation process.[32] For example, the lattice mismatch of CdS and Ag_2S can induce the spontaneous formation of periodic structures in colloidal nanorods[29] and cation vacancies in Cu_2Se can direct the formation of a Janus-like heterostructures made of immiscible Cu_2Se and ZnSe domains.[30] When several chemical transformation methods are employed simultaneously, the relation to the initial atomic structure can be more complicated.[33] Therefore, understanding the structural mechanisms of the different postsynthetic reactions are critically important for elucidating "nanosize" effects and for tailoring nanomaterial properties.

The ion exchange method is a common route to change the parent nanomaterial's chemical composition.[34,35] Both the cation and anion can be exchanged to introduce new elements through substitution of the original ions, with potentially beneficial outcomes.[33] The driving force for cation exchange is a balance between the solvation energy of the cations and the binding energy for the lattice,[34] while the realization of anion exchange can be explained by the theory of mass action and reaction thermodynamics, which are associated with the concentration and activation of the starting reagents, respectively.[36,37] Of these two methods, cation exchange is more widely used in the transformation of nanocrystals because of its faster kinetics.[38] Moreover, the appropriate kinetics for cation exchange open the possibility to form kinetic products and to metastable phases.[39] Another effective method for structural transformation is the redox reaction, which is commonly applied to convert the metallic nanocolloids to other binary semiconductors like oxides, sulfides, or phosphides.[2,20,40] Beyond the apparent compositional transformation, the redox reaction often results in nanomaterials with a hollow structure due to the nanoscale Kirkendall effect.[20] Surface treatments, such as ligand exchange and ligand etching, also induce CTNs. The organic ligands are an integral part of colloidal nanocrystals and nanoclusters, and they can demonstrate a variety of binding modes to the inorganic surface.[41] Ligand exchange is a way to engineer the surface structure of the parent nanocolloid, which can induce structural changes in the core.[42,43] Additionally, the organic−inorganic interactions can bring about ligand etching to the inorganic materials, and this is particularly interesting for nanocrystals with a heterostructure, where the etching process can selectively etch a specific compositional domain dependent on its atomic structure.[3] Chemical transformation of nanocolloids can be broadly separated into two distinct size categories, nanocrystals (above 2 nm) and nanoclusters (below 2 nm).[44] Transformation reactions can greatly differ for these two classes of materials, with the reasons behind these differences still unclear.

In this Account, we will highlight the different routes to manipulate the structure and chemistry in nanocolloids through CTNs, and, equally, we will examine how the atomic structure in the nanocolloids directs the CTN pathways. We will show how the atomic structural differences in nanocluster systems compared to nanocrystals can be responsible for the radically different effects of chemical transformations. While

https://dx.doi.org/10.1021/acs.accounts.0c00704
Acc. Chem. Res. 2021, 54, 509−519

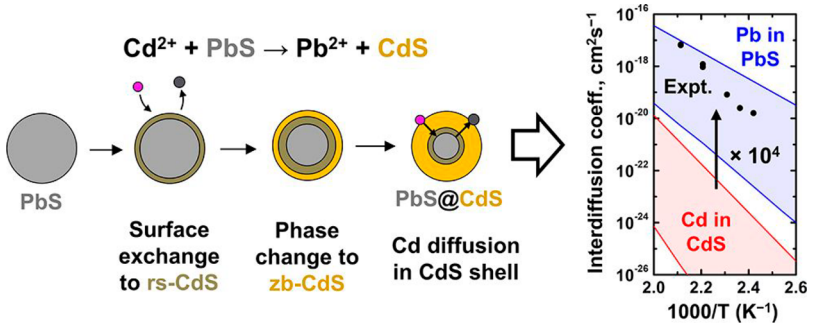

Figure 1. Schematic of cation exchange of PbS into CdS and accompanying interdiffusion coefficient data from in situ XRD experiments and reference values for Cd in CdS and Pb in PbS. Interdiffusion is found to be 10^4 larger than bulk values.

there is an abundance of impressive, published literature on CTNs, we will feature the small subset of results from our lab and focus on the interconnection between chemically induced CTNs and atomic structure.

2. CHEMICAL TRANSFORMATIONS IN NANOCRYSTALS: A PLATFORM FOR A WELL-CONTROLLED STRUCTURE AND MORPHOLOGY ENGINEERING

2.1. Overview

Nanocrystals, with a size range between 2 and 100 nm, comprise an ideal platform to postsynthetically manipulate structure and composition, and to isolate metastable structures.[45] Compared with their bulk analogs, the morphology, composition, and atomic structure of nanocrystals can be facilely engineered through simple chemical inductions. Unlike the smaller nanoclusters (<2 nm), the products of chemical transformations on nanocrystals can be stabilized in partially transformed states.[46] This ability for partial transformations enables structures that are kinetically metastable, and, given the finite number of atoms and the accelerated speed of the reactions, it enables atomic organizations that are inaccessible in larger systems. The postsynthetic methods for the nanocrystal transformation include ion exchange (cation and anion exchange),[34,35,47] redox reaction,[40] and ligand treatment.[48] By elaborately tuning these reactions, novel materials with useful applications can be stabilized.

2.2. Cation Exchange

Among the postsynthetic methods to manipulate parent nanocrystals, the cation exchange reaction is the most popular soft chemistry approach.[26,49] Cation exchange is a postsynthetic reaction in which cations in the host nanocrystal are substituted (exchanged) by cations in solution. The driving force behind these exchanges is solvation, meaning that the parent cation is more soluble in solution than in the solid.[31] Importantly, the anion framework often provides stability that enables the overall morphology of the nanocrystal to be maintained through the cation exchange.[50] Cation exchange will often induce a solid−solid phase transformation in the nanocrystals, which can be tuned to form novel structural/compositional changes such as the formation of heterostructure or core−shell architectures, making cation exchange an emerging and effective way to accurately tailor function materials.[1]

Cation exchange initiates through surface chemistry on the mother nanocrystal, inducing the phase transformation at the interface of the heterolayer.[28] Although the final product can be easily characterized, one of the mysteries surrounding the reaction is the structural and kinetic pathway that occurs during the transformation. In the original Alivisatos et al. paper on cation exchange, they noted that the kinetics were faster than what could be expected from scaling bulk processes.[21] But monitoring the kinetics in such a dynamic process is challenging, and characterizing the time scales and diffusion constants has eluded the community. In our lab, we were recently able to quantify the kinetics by using *in situ* X-ray diffraction (XRD) for the exchange reaction PbS + $Cd(oleate)_2$ → PbS@CdS (core@shell architecture) + $Pb(oleate)_2$.[51] By monitoring the phase change in this model system, we found that the exchange reaction proceeds through three different stages: (1) formation of metastable CdS rock salt structure, (2) recrystallization of the CdS rock salt phase into zincblende structure, and (3) diffusional growth of zincblende CdS. Among these three stages, the diffusion-controlled growth of the zinc-blended CdS is the rate-limiting step with an activation energy of around 160−180 $kJ{\cdot}mol^{-1}$, which substantially exceeds those reported before but is similar to bulk values. Most surprising are the measured interdiffusion coefficient which is more than 10 000× larger than the self-diffusion coefficients of the slowest component (Cd in CdS) (Figure 1). The findings suggest that the very large chemical potential gradient accelerates the diffusion rate within the nanocrystal and there is likely a link to the number of unit cells comprising the atomic phase, but the exact mechanism is not yet clear. This work shows that the driving forces in nanosystems can be substantially different from bulk materials during cation exchange, and could lead to novel structural rearrangements.

Cation exchange reactions begin as a single-domain nucleation event (driven by thermodynamics) on the surface of a nanocrystal that can then initiate a solid−solid transformation.[39] As the phase transformation propagates through the material, its growth is dependent on the localization of the surface event, the different coverage of the surface facets by ligands, and the atomic crystal structure. All of these parameters can lead to anisotropies resulting in heterostructure formation through the phase transformation.[29] Equally important to the phase is the influence of the diffusing species and the interfacial topotaxy in the heterostructure. We used copper sulfide ($Cu_{2-x}S$, $0 \le x \le 1$) nanocrystals as our platform to investigate solid−solid transformations and heterostructures nanocrystals.[1] In this study, Zn^{2+} was introduced as the guest ion for cation exchange. Because the crystal structure is anisotropic along one direction in the parent phase, the cation exchange with Zn^{2+} introduces a dual-

https://dx.doi.org/10.1021/acs.accounts.0c00704
Acc. Chem. Res. 2021, 54, 509−519

interface heterostructure in free-standing nanocrystals (Figure 2). Two competing processes control the phase of the copper sulfide: the exchanged species diffusing out of the ZnS layers, and the interfacial strain force.

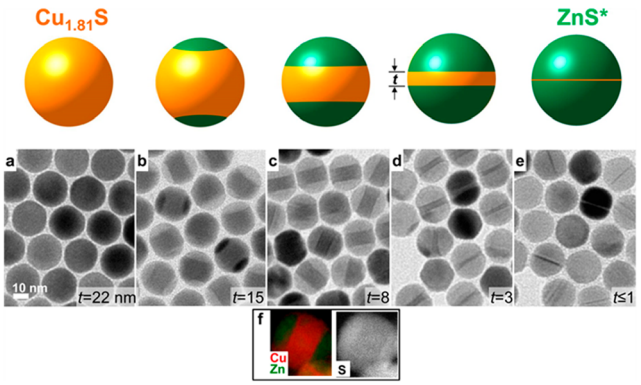

Figure 2. Cation exchange transformation of copper sulfide NCs into dual-interface heterostructured particles with zinc sulfide caps. Schematic (top) and transmission electron microscopy (TEM) images (bottom) show the composition change from the initial copper sulfide particle (a, leftmost) into ZnS* (e, rightmost). The final product is denoted ZnS* because a thin 2D copper sulfide disk is present in the TEM images for ∼30% of the NCs. The copper sulfide disk thickness (t) is indicated. (f) STEM-EELS (scanning TEM coupled with electron energy loss spectroscopy) image showing the presence of Cu and Zn (left) and S (right) in the heterostructured particles.

Before cation exchange, the parent $Cu_{2-x}S$ phase is copper-deficient, with a $Cu_{1.81}S$ roxbyite atomic structure. The introduction of Zn^{2+} creates a dual-interface 'nanohamburger' geometry with the ZnS grains forming at opposite ends of the spherical nanocrystals (Figure 3). Both X-ray diffraction and

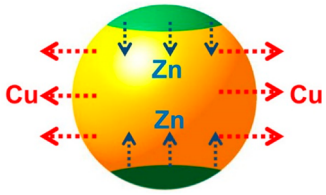

Figure 3. Diffusion pathways of Cu and Zn atoms during the cation exchange reaction in heterostructured nanocrystals. On the basis of calculated diffusion activation barriers, during the cation exchange the Zn diffuses inward from the ZnS regions (green) and the Cu diffuses in the Cu−S region (orange). The excess Cu in the Cu−S region could be the cause for the solid−solid phase transformation.

electron microscopy analysis indicate that a tertiary Cu−Zn−S phase is not present and, instead, an atomically sharp heterostructure interface is formed. The onset of the cation exchange process immediately initiates a phase transformation of the roxbyite-type $Cu_{1.81}S$ to the thermodynamically more stable djurleite ($Cu_{1.94}S$)/low chalcocite (Cu_2S), through the diffusion of the exiting Cu ions: density functional theory (DFT) shows that the diffusion pathway for the Cu in the $Cu_{2-x}S$ phase is greatly favored compared to the ZnS phase (Figure 2). But as the cation exchange reaction proceeds and the thickness of the copper sulfide layer reduces, the low-energy copper sulfide phase transforms back to the initial roxbyite type structure, which then becomes the dominate phase when the copper sulfide disk is ∼10 nm or less in thickness. This phase reversal can be explained by the increasing strain energy from the interface: continuum modeling calculations of the strain distributions in the heterostructured nanocrystals reveal the strain energy density increases as the copper sulfide layer thickness decreases (Figure 3) and a maximum (8.5×10^{-21} J·nm^{-3}) is reached when t = 4.8 nm. The strain is a result of the mismatch of between the djurleite/low chalcocite phase and the ZnS atomic structure. When the strain energy reaches to a critical value, it forces the phase to transform back to the better-matched roxbyite lattice to minimize the strain energy. This work shows that the structure can direct the cation exchange reaction to form anisotropic exchange interfaces and, in turn, the phase can be directed by the cation exchange through the diffusion of cations and the extent of the domain size.

2.3. Anion Exchange

The exchange of anions is another important postsynthetic approach to restructure a parent nanocrystal. Compared with the cation exchange method, however, the replacement of the anion is much more difficult due to the lower reaction efficiency caused by the larger anionic radii, which results in a low ion diffusion rate.[37] Also, the high energy barrier for the rearrangement of the anionic framework (formation of anionic vacancies and recombination of guest anion with cations) is another factor that hinders the anion exchange process.[47] Despite these challenges, encouraging work has demonstrated the power of this method for the preparation of novel nanomaterials. For example, the solution-based anion exchange reactions have been developed by Schaak and Dawood[52] and Alivisatos *et al.*,[53] in which the ZnO nanocrystals can be effectively converted to ZnS by employing thiourea and (trimethylsilyl)-sulfide (TMS). These works clearly emphasize the importance of a highly reactive anion precursor to increase the reaction efficiency and achieve anion exchange, however both precursors required relatively high temperature conditions (>150 °C).

Our group has demonstrated that the ammonium sulfide ($(NH_4)_2S$) is a highly reactive sulfide precursor capable transforming the anion lattice while maintaining the entire nanocrystal form at a low temperature (Figure 4).[54] In these

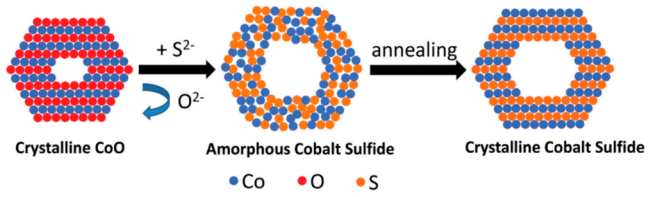

Figure 4. Schematic illustration of the chemical transformation from CoO to cobalt sulfide nanocrystals by anion exchange.

experiments, the initial hollow CoO nanocrystals are readily converted to Co_3S_4 within 5 min at 70 °C after the addition of a $(NH_4)_2S$-oleyamine solution. Because of the slow diffusion of the anions, the structural backbone of the crystal is disturbed if the reaction continues toward completion. In the CoO system, the anion exchange leads to amorphous Co_3S_4 for full exchange reactions. Another structural effect in this system from anion exchange is the expansion of the hollow core. While the overall morphology is maintained, after the reaction with $(NH_4)_2S$, the average particle size increases from 14.4 to 16.4 nm and the

https://dx.doi.org/10.1021/acs.accounts.0c00704
Acc. Chem. Res. 2021, 54, 509−519

void increases from 6.3 to 11.9 nm. The expansion of the void can be ascribed to the faster diffusion rates of Co^{2+} and O^{2-} than the incoming S^{2-}.

Partial anion exchange can be used to preserve the structural framework and can capture kinetic products, which can have advanced properties beyond the parent nanocrystals. For example, in the CoO → CoS_x system, we isolated a series of partial anion exchange cobalt oxysulfide products and tested their activity as hydrogen evolution reaction (HER) electrocatalysts (Figure 5).[55] We found that a light sulfur substitution

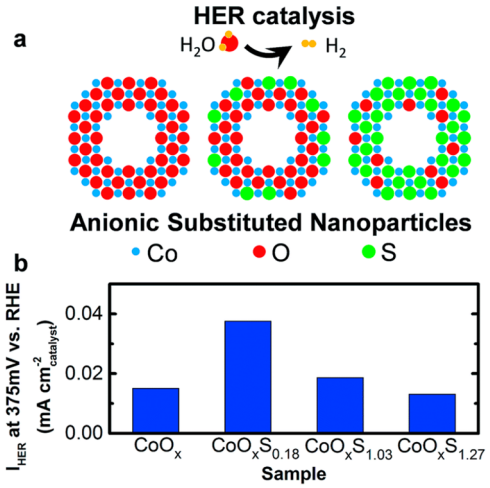

Figure 5. Schematic of the anionic substitution in CoO_x nanoparticles as a testbed for HER electrocatalysis (a). Results from this work indicate that the maximum HER activity occurs at low doping levels (*e.g.*, $CoO_xS_{0.18}$), while at higher doping levels activity decreases (b).

yields a metastable, distorted S-substituted CoO phase ($CoO_xS_{0.18}$) that exhibits HER catalytic activity that is 2−3 times more active than that of either end-member of the substitution series.

2.4. Redox Reaction

A more aggressive route to realize nanocrystal transformation is redox reaction, in which parent metallic nanocrystals are transformed into binary compounds like oxides or sulfides, through a redox reaction.[40] During these processes, a diffusion couple is formed between the guest anions diffusing inward and the host cations diffusing outward. If the diffusion rates are asymmetric in the diffusion couple, the structure and morphology of the nanocrystals is greatly affected. Most famously, the nanoscale Kirkendall effect is the hollowing of nanomaterials, which can take place during a redox reaction as well as during other chemical transformations that involve in/outward ion diffusion process with different diffusion rates.[53,54,56,57] Therefore, insight into the diffusion mechanism is a central task to understand the redox addition.

Our lab has investigated the relationship between atomic structure and the nanoscale Kirkendall effect by examining the intermediate products in two model systems: the conversion of ε-Co to CoP_x[2] and ε-Co to CoO_x.[40] These reactions involve the oxidation of the metallic cobalt into either phosphides or oxides. Researchers had previously believed that the Kirkendall-hollowing was a straightforward one-step mechanism in nanocrystals, directly related to the bulk Kirkendall effect.[20] From our studies, we found that the nanoscale Kirkendall effect is a two-step process that is linked to the atomic structure: first, a metastable amorphous shell material forms, the amorphous layer then crystallizes and at that point the rates in the diffusion couple are inverted, resulting in the hollowing.

For cobalt oxide system, the initial metallic cobalt nanocrystals are first oxidized into an amorphous CoO intermediate phase and then transformed to the final hollow Co_3O_4 nanocrystals. At different transformation stages, the rates for the inward (O) and outward (Co) diffusions change. Through experimental characterization and theoretical calculation, it was shown that O diffuses faster than Co in the ε-Co structure during the first stage, allowing O to enter the ε-Co particle to produce the amorphous CoO. Once the CoO crystallizes, the fastest diffusion species switches from O to Co, yielding hollow Co_3O_4 nanocrystals. This two-step mechanism correlates well with experimental results showing that the center void only begins to appear after 5−10 min of the reaction. An identical process is observed in the phosphidation of cobalt to produce the hollow CoP nanocrystals. With the tri-*n*-octylphosphine (TOP) as the phosphorus source, the P's inward diffusion dominates at the beginning and an amorphous Co−P shell is formed on the surface. After the shell crystallizes into the Co_2P phase, the P anion lattice becomes immobile and the outward diffusion of Co is faster than the inward diffusion of P. Figure 6

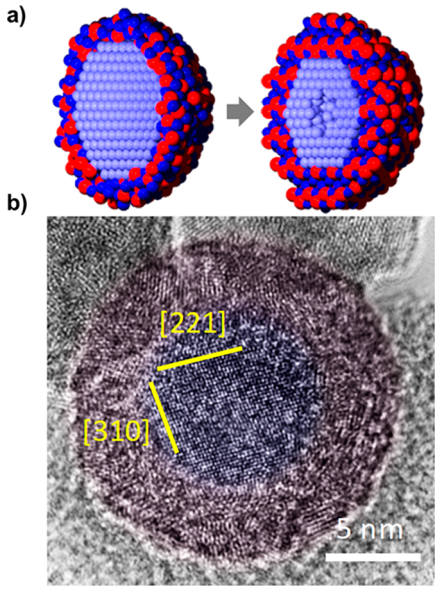

Figure 6. (a) Evolutional schematics of transition from cobalt to cobalt phosphide nanocrystals. (b). High resolution TEM image of the intermediate NC between ε-Co and Co_2P. The core shows ε -Co phase as indicated by the (221) and (310) lattice planes.

shows the first step (metastable shell) as captured with high-resolution transmission electron microscope images. Both of these examples demonstrate how the redox and diffusion processes leading to the nanoscale Kirkendall effect are critically dependent on atomic structure.

2.5. Ligand Etching

Solid-state transformation of nanocrystals can also be realized through chemical process at the solid-solution interface, namely the organic ligand-inorganic surface interaction.[58] It has been well-established that the surfactant ligands are able to demonstrate a variety of binding modes to the inorganic surface, depending on the binding group.[41] But the binding

https://dx.doi.org/10.1021/acs.accounts.0c00704
Acc. Chem. Res. 2021, 54, 509−519

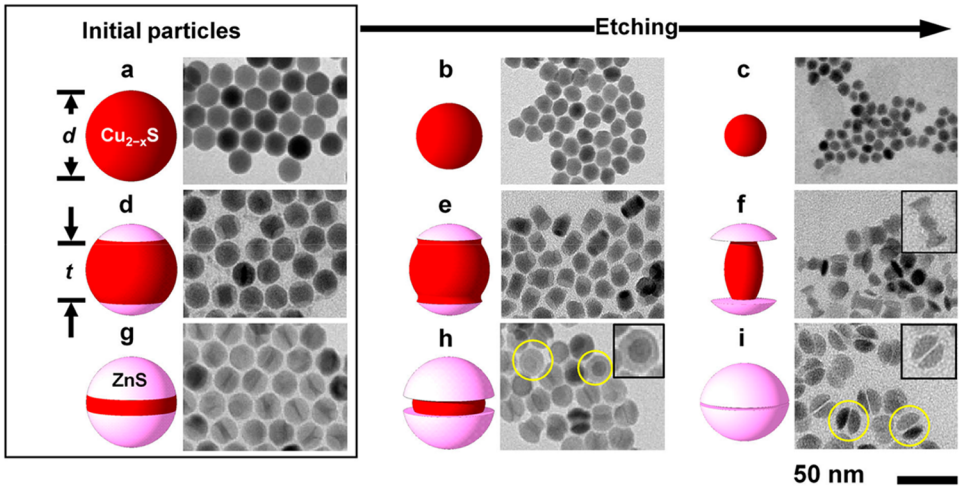

Figure 7. Schematic and TEM images of the etching of $Cu_{2-x}S$ pure nanocrystals (SC-NCs; a–c) and $Cu_{2-x}S$-ZnS heterostructures (H-NCs; d–i) by trialkylphosphines. SC-NCs are slowly reduced in diameter, d, from $d \sim 22$ nm (a) to $d \sim 17$ nm over 17 h (b) and to $d \sim 12$ nm over 48 h (c). For H-NCs, $Cu_{2-x}S$ is removed with nearly perfect selectivity: with an initial $Cu_{2-x}S$ thickness $t = 15$ nm (d), the heterostructure takes on the appearance of a thick nanorod with ZnS tips after 15 min (e); eventually, the $Cu_{2-x}S$ layer is reduced to a thin rod (f); a fraction of the particles have slightly enlarged centers (inset). For an initial $t = 4$ nm (g), etching of the $Cu_{2-x}S$ layer is apparent after 2 min (h). A fraction of the particles (circled in yellow) have a c-axis parallel to the electron beam, showing that the etching is radially isotropic (h, inset). After 1 h, $Cu_{2-x}S$ is completely removed (i), leaving apparently connected ZnS caps (i, inset); a few pairs of particles (circled) show different levels of contrast, indicating that they display different angles to the electron beam due to postsynthetic rotation of the initially epitaxial grains.

interactions can also initiate structural transformations and lead to the dissociation of the inorganic lattice, or ligand etching. We recently found that the ligand etching process can have atomic specificity, in which the organic ligand demonstrates a preference for etching a specific inorganic species.[3] In ZnS-$Cu_{2-x}S$ heterostructures, the trialkylphosphine ligand shows a selective etching of the $Cu_{2-x}S$ component while the ZnS remains untouched (Figure 7). The etching patterns can be tuned between isotropic and basal-plane directed etching by changing the phosphine concentration. Structurally, the trialkylphosphines destabilize the $Cu_{1.81}S$ roxbyite lattice: the phosphines induce a phase transformation by "injecting" Cu atoms into and removing S from the $Cu_{2-x}S$, converting it into a copper-rich phase, and this destabilization is mediated by the amount of strain in the copper sulfide layer. The preferential compositional etching on $Cu_{1.81}S$ can be explained by the presence of the S^- in $Cu_{2-x}S$ structure, which is more easily oxidized and removed by phosphine, while the more ionic ZnS phase only contains S^{2-}. Structurally, the defect-tolerant $Cu_{2-x}S$ phases are able to stabilize the excess Cu cations by depleting the vacancy population. The ZnS structure is much less tolerant of vacancies. Thus, the vacancy-rich atomic structure of the $Cu_{2-x}S$ phases is a key enabler to the chemical transformation by ligand etching, resulting in a solid–solid phase transition.

3. CHEMICAL TRANSFORMATION IN NANOCLUSTERS: MOLECULAR-LIKE BEHAVIOR

3.1. Overview

Compared with the relatively larger nanocrystals, nanoclusters are smaller (<2 nm) and consist of a limited number of atoms, and their atomic structure and stoichiometry need not be the same as those of their bulk analogues.[44] Because of the relatively high fraction of surface atoms, nanoclusters can react transform very differently than nanocrystals to chemical treatments. One of the most obvious differences is that the nanoclusters can behave like small molecules during chemical transformations.[59,60] For example, solvent exchange can trigger an icosahedral-to-cuboctahedral structural transformation for Au_{13} nanoclusters[61] and ligand exchange can be used for reversible structural transformations in Pt_1Ag_{28} nanoclusters.[62] Moreover, doping cations can easily reach to the core section of the nanocluster due to their ultrasmall size.[63] A subfamily of nanoclusters is magic size clusters (MSCs), called "magic" because they exhibit intrinsic resistance to crystal growth by conventional single-atom addition and instead grow in discrete spurts between stable magic sizes.[64] MSCs are atomically identical in chemical composition and structure. The synthesis of high purity MSCs, unfortunately, is not trivial work. Although several different cluster families, such as F309, F311, F313, F324, F348, F360, and F378 (denoted based on the position of their distinctive exciton peak), have been reported so far,[64−70] the mixture of other phases and the coexistence of large nanocrystals make the rigorous research of MSCs problematic. In order to address this issue, we developed a robust solventless synthesis (high-concentration) synthetic approach that produces high-purity oleic-acid-caped CdS MSCs in a large yield.[71] The key in this method is to run the reaction in a high concentration condition to facilitate the formation of an ordered organic–inorganic mesophase in solution. The mesophase confines the nanocrystal growth and stabilizes the MSCs, protecting them from further growth (Figure 8). The CdS MSCs are ~1.5 nm, belonging to the F324 family with a single, narrow (the full width at half-maximum ≈7.5 nm or 87 meV) absorption peak at 324 nm. The lack of lower-energy exciton peaks indicates that the MSCs have purity >99.9%, which translates to a selectivity that is 2 orders of magnitude more pure than comparative studies.

3.2. Irreversible Transformation through Ligand Exchange

The optoelectronic properties of nanomaterials are inherently correlated to the complex physiochemical interactions between the organic ligands and inorganic core.[72] Through a ligand exchange process, colloidal nanomaterials can undergo phase

https://dx.doi.org/10.1021/acs.accounts.0c00704
Acc. Chem. Res. 2021, 54, 509–519

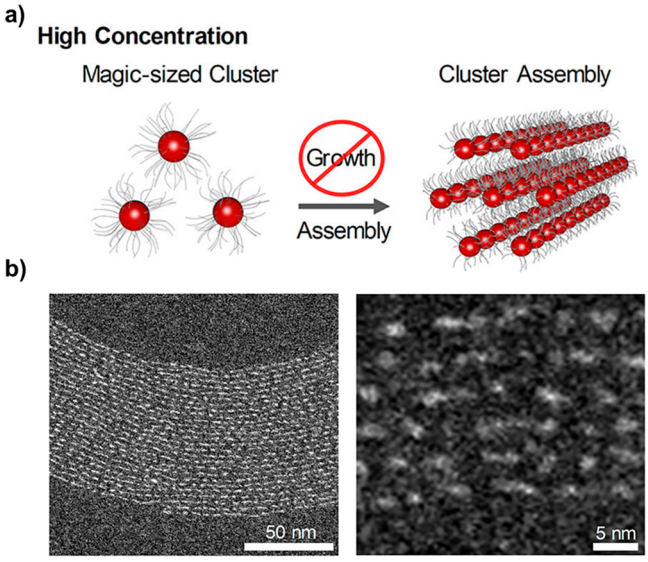

Figure 8. (a) Schematic illustration showing the formation of mesophase assembly prevents MSCs from growing into large NCs. (b) High resolution STEM of MSCs.

transformation, displaying significant shifts for the characteristic exciton peak. Compared with the traditional nanocrystals (NCs), the small MSCs have higher sensitivity in response to these chemical treatments. We reported that the F324 can be readily converted to F348 and F360 via ligand exchanges with 1-dodecanethiol and *n*-butylamine, respectively, characterized by their respective absorption peaks (Figure 9).[42] The chemical treatment of F324 with methanol results in a blue-shift of the absorption peak to 313 nm, which represents molecular addition instead of ligand exchange.[4] Larger CdS NCs, however, are inert to the same ligand and chemical treatments, maintaining identical excitonic peak positions after ligand exchange.

Chemical and structural analyses provide insight into how differently the MSCs and NCs respond to these surface treatments. Compositional analysis by inductively coupled plasma optical emission spectrometry (ICP-OES) and thermogravimetric analysis (TGA) finds that the initial F324 MSCs are cadmium rich, with a nearly 2:1 ratio of Cd to S. This departs greatly from typical stoichiometries in NCs and has implications for the atomic structure and surface sites. Additionally, the methanol-treated F324 remains compositionally identical to the initial F324, while the F360 shows a decreased Cd:S ratio, indicating a loss of cadmium atoms that is consistent with L-promoted Z-type ligand displacement. The compositional analysis of the F348 is complicated by the presence of sulfur atoms in both inorganic core and organic ligands, but generally finds that two thiol ligands are added to the MSC per surface cadmium. XRD indicates that the initial F324 has a wurtzite type structure whereas the surface-modified F313, F348, and F360 feature a zinc blended structure. Based on Fourier transform infrared (FTIR) spectroscopy, the initial capping ligands of oleic acid are completely replaced with thiol and amine for both the MSCs and NCs, while, in the case of methanol, the methanol molecule is just added onto the surface without peeling off the original organic ligands.

In summary, the ultrasmall size of the MSCs promotes a different response to chemical transformations compared to

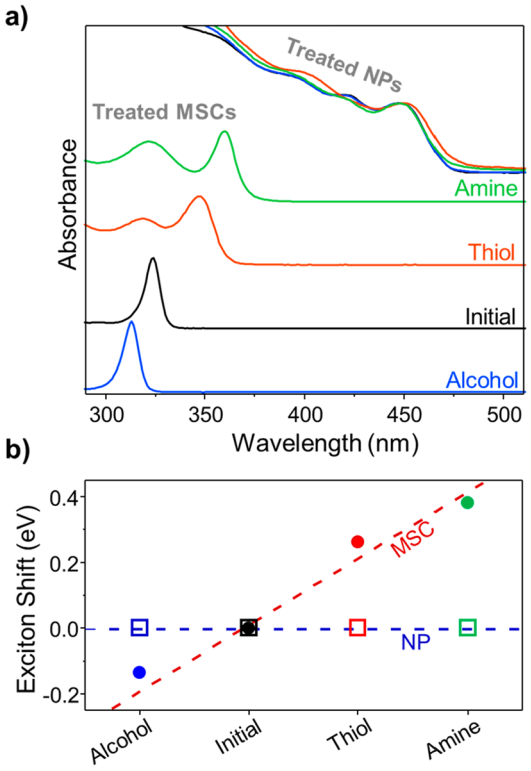

Figure 9. (a) Absorption spectra of high-quality MSCs and NCs. Each family is derived from the 324 nm family (F324 or Initial) by a chemical treatment. Alcohol, thiol, and amine treatment produce, respectively, F313, F348, and F360. There is no significant change in the excitonic position of the NCs for each treatment. (b) Comparison of the shift of the lowest energy excitonic peak relative to the initial sample for MSCs and NCs.

the slightly larger nanocrystals. The response can be traced to differences in atomic structure and composition between the sizes, and that MSCs have heightened surface-sensitivity due to their larger fraction of surface atoms. Additionally, this work shows that whereas NCs most often undergo a continuous transformation process, certain transformations in MSCs occur in distinct states. Such well-defined, discrete states are especially useful for switch applications, such as sensors.

3.3. Reversible Isomeric Transformation through Chemical Treatment

The purity and structure of our CdS MSCs have illuminated previously unseen connections between large and small structural phase transitions.[42] For years, scientists have been trying to discover the size at which solid materials could change their internal structure in a single, swift step, like molecules do during isomerization.[8] Molecular isomerization and solid−solid transformations conceptually represent structural transformations at two length scale extremes (small molecules and extended solids) but arise from the same principles: preservation of the overall system composition. The continuous deformation that defines the solid−solid transformation sharply contrasts that of the discrete transition exhibited by a molecular isomerization, which poses the question: at what length scale do these transformations become mechanistically identical? This question was answered when the first reversible chemically introduced isomerization was discovered in the aforementioned magic size cluster F324.[4] With the assistance of the pair distribution function (PDF)

https://dx.doi.org/10.1021/acs.accounts.0c00704
Acc. Chem. Res. 2021, 54, 509−519

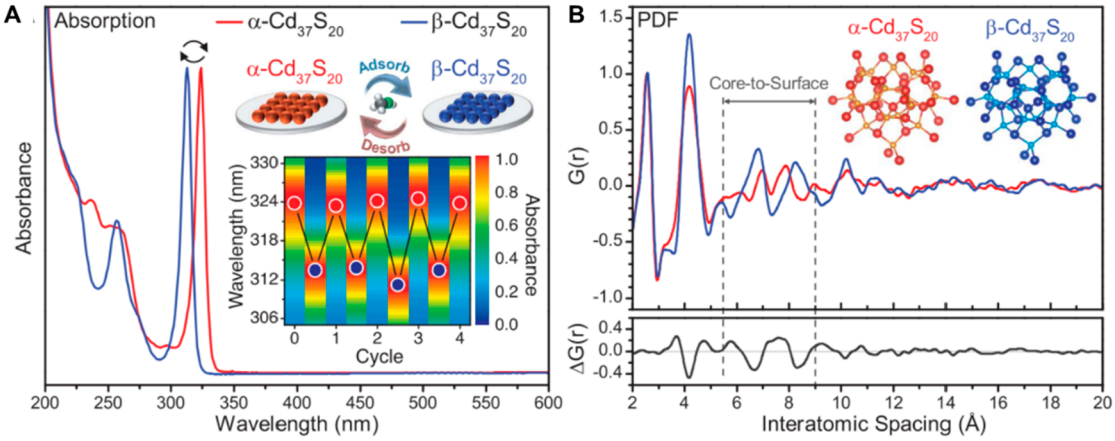

Figure 10. (A) Absorption spectra of pristine cluster isomers α-$Cd_{37}S_{20}$ and β-$Cd_{37}S_{20}$, with excitonic peaks at 324 and 313 nm, respectively. The two isomers switch reversibly upon alcohol adsorption and desorption (inset schematic and contour plot). (B) PDFs of the a and b isomers. $\Delta G(r) = \Delta G_{\alpha}(r) - G_{\beta}(r)$ is the difference in the PDF between the two isomers and is largest for core-to-surface atom pair distances. Inset are the fitted structures of the α and β isomers with residuals of ~0.18.

analysis and reverse Monte Carlo algorithms, the atomic structure of the clusters is found to be $Cd_{37}S_{20}$ in one of two distinct atomic configurations (α or β phase). These two different atomic structure configurations are switchable upon absorption/desorption of water or alcohol (hydroxyl groups) with an activation barrier of ~1 eV in both directions, displaying sharp and distinct characteristic absorption peaks at 324 nm (α-$Cd_{37}S_{20}$) and 313 nm (β-$Cd_{37}S_{20}$) (Figure 10). The kinetics demonstrate single-exponential interconversion of discrete transitions between the two cluster isomers, as in molecular isomerization. Structure analysis definitively reveals a displacive rather than reconstructive reconfiguration of the clusters, characteristic of a diffusionless solid−solid transformation. The isomerization from α- to β-type $Cd_{37}S_{20}$ is initiated from the surface structure reconfiguration when the alcohol molecules are adsorbed, and the reverse process can be achieved by heating to remove the alcohol. FTIR spectroscopy indicates that the absorption/desorption of the alcohol molecules changes the binding patterns for the carboxylic ligands from mainly bridging to chelating in the α- and β-MSCs, respectively. Such changes further trigger a reconfiguration of surface Cd and S atoms and thereby propagate throughout the entire Cd−S lattice of the inorganic cluster. The mechanism for the transformations can be linked directly to the atomic structure and its divergence from bulk structure. While large nanocrystals have bulk-like, extended atomic structure that is constructed from infinite arrangements of symmetric tetrahedral subunits, the MSC is composed of a nonsymmetric packing of distorted tetrahedral units. The atomic arrangement in these MSCs also explain why isomerization has not been identified in other CdS clusters with bulk-like structure.

4. CONCLUSIONS AND OUTLOOK

Nanocrystal and nanocluster chemical transformation represents an important dynamic process, allowing one to design new functional materials that cannot be directly prepared through conventional synthetic methods. The richness of the transformation patterns gives rise to a great variety of nanomaterials with different chemical compositions, atomic structures, and morphologies. Unveiling the secrets that govern the transformation process is necessary to predict the transformation's outcomes and rationally design methodologies. In this Account, we have shed light on the interrelationship between the atomic structure and chemical transformations and on how atomic structure differences for different characteristic length scales (small nanoclusters <2 nm and large nanocrystals 2−100 nm) create different driving forces for the chemically induced phase transformations. The larger nanocrystal system has a stable rigid framework that allows a continuous phase evolution in which many interesting, metastable intermediate compounds become accessible. Additionally, the transformation can be confined in a specific domain of the nanocrystals, such as the cap or surface, which provides an accurate means to engineer the nanomaterials in order to achieve the desired properties. On the other hand, ultrasmall nanoclusters demonstrate a different transformation pathway upon chemical treatment. Due to the nonstandard arrangement distorted tetrahedral units, nanoclusters can behave like molecules with a discrete and, more intriguingly, reversible transformation.

Although a clear difference of the nanocrystal transformation can be seen for the large nanocrystals and small nanoclusters, one outstanding question still remains: what is the critical size that separates the transformative nanocrystals into these two different families? It is possible that the critical size may vary depending on the composition or transformation conditions. Further, nanoclusters themselves may show size-dependent transformation patterns. Therefore, answering these questions will help to gain deeper insights into the mechanism and better controls in the smart design of new materials for real applications.

AUTHOR INFORMATION

Corresponding Author

Richard D. Robinson − *Materials Science and Engineering Department, Cornell University, Ithaca, New York 14853, United States;* orcid.org/0000-0002-0385-2925

Authors

Haixiang Han − *Materials Science and Engineering Department, Cornell University, Ithaca, New York 14853, United States;* orcid.org/0000-0002-8465-9624

https://dx.doi.org/10.1021/acs.accounts.0c00704
Acc. Chem. Res. 2021, 54, 509−519

Yuan Yao − *Materials Science and Engineering Department, Cornell University, Ithaca, New York 14853, United States;* orcid.org/0000-0002-4784-2753

Complete contact information is available at: https://pubs.acs.org/10.1021/acs.accounts.0c00704

Author Contributions

†H.H. and Y.Y.: Equal contribution.

Notes

The authors declare no competing financial interest.

Biographies

Haixiang Han is a Postdoctoral Research Associate in the department of Materials Science and Engineering at Cornell University, in the group of Richard Robinson. He received his B.S. in applied chemistry from Shandong Agricultural University and his Ph.D. in inorganic chemistry from the University at Albany, State University of New York in 2018. His research interests are the design, synthesis, and application of chiral nanoclusters and their assembly.

Yuan Yao is a Ph.D. candidate in the department of Materials Science and Engineering at Cornell University, in the group of Richard Robinson. He received his B.S. from University of Manchester in 2016 and his M.S. from Cornell University in 2018. His research interests include synthesis of ternary metal sulfide nanoparticles and understanding plasmonic behavior in intermediate band semiconductors.

Richard Robinson is an Associate Professor in the department of Materials Science and Engineering at Cornell University. He earned his B.S. and M.S. in Mechanical Engineering from Tufts University, his Ph.D. in Applied Physics from Columbia University in 2004, and was a postdoctoral fellow at U.C. Berkeley/LBNL with the Alivisatos group, before joining Cornell. His research interests are in understanding and controlling light−matter interactions, chemical transformations in nanocrystals and nanoclusters, and synchrotron X-ray characterization of nanomaterials.

■ ACKNOWLEDGMENTS

This work was supported in part by the National Science Foundation (NSF) under Award Nos. CHE-1507753 and DMR-2003431. This report includes work made use of the Cornell Center for Materials Research Shared Facilities, which are supported through the NSF MRSEC (Materials Research Science and Engineering Centers) program (Grant DMR-1719875 and DMR-1829070). This report includes research conducted at the Cornell High Energy Synchrotron Source (CHESS), which is supported by the NSF and the National Institutes of Health−National Institute of General Medical Sciences under NSF award DMR-1332208 and DMR-1829070.

■ REFERENCES

(1) Ha, D.-H.; Caldwell, A. H.; Ward, M. J.; Honrao, S.; Mathew, K.; Hovden, R.; Koker, M. K. A.; Muller, D. A.; Hennig, R. G.; Robinson, R. D. Solid−Solid Phase Transformations Induced through Cation Exchange and Strain in 2D Heterostructured Copper Sulfide Nanocrystals. *Nano Lett.* **2014**, *14* (12), 7090−7099.

(2) Ha, D.-H.; Moreau, L. M.; Bealing, C. R.; Zhang, H.; Hennig, R. G.; Robinson, R. D. The Structural Evolution and Diffusion During the Chemical Transformation from Cobalt to Cobalt Phosphide Nanoparticles. *J. Mater. Chem.* **2011**, *21* (31), 11498−11510.

(3) Nelson, A.; Ha, D.-H.; Robinson, R. D. Selective Etching of Copper Sulfide Nanoparticles and Heterostructures through Sulfur Abstraction: Phase Transformations and Optical Properties. *Chem. Mater.* **2016**, *28* (23), 8530−8541.

(4) Williamson, C. B.; Nevers, D. R.; Nelson, A.; Hadar, I.; Banin, U.; Hanrath, T.; Robinson, R. D. Chemically Reversible Isomerization of Inorganic Clusters. *Science* **2019**, *363* (6428), 731−735.

(5) Zaziski, D.; Prilliman, S.; Scher, E. C.; Casula, M.; Wickham, J.; Clark, S. M.; Alivisatos, A. P. Critical Size for Fracture during Solid−Solid Phase Transformations. *Nano Lett.* **2004**, *4* (5), 943−946.

(6) Kovalenko, M. V.; Manna, L.; Cabot, A.; Hens, Z.; Talapin, D. V.; Kagan, C. R.; Klimov, V. I.; Rogach, A. L.; Reiss, P.; Milliron, D. J.; Guyot-Sionnnest, P.; Konstantatos, G.; Parak, W. J.; Hyeon, T.; Korgel, B. A.; Murray, C. B.; Heiss, W. Prospects of Nanoscience with Nanocrystals. *ACS Nano* **2015**, *9* (2), 1012−1057.

(7) Wittenberg, J. S.; Miller, T. A.; Szilagyi, E.; Lutker, K.; Quirin, F.; Lu, W.; Lemke, H.; Zhu, D.; Chollet, M.; Robinson, J.; Wen, H.; Sokolowski-Tinten, K.; Alivisatos, A. P.; Lindenberg, A. M. Real-Time Visualization of Nanocrystal Solid−Solid Transformation Pathways. *Nano Lett.* **2014**, *14* (4), 1995−1999.

(8) Chen, C.-C.; Herhold, A. B.; Johnson, C. S.; Alivisatos, A. P. Size Dependence of Structural Metastability in Semiconductor Nanocrystals. *Science* **1997**, *276* (5311), 398.

(9) Zou, X.; Wang, P.-P.; Li, C.; Zhao, J.; Wang, D.; Asefa, T.; Li, G.-D. One-Pot Cation Exchange Synthesis of 1D Porous CdS/ZnO Heterostructures for Visible-Light-Driven H_2 Evolution. *J. Mater. Chem. A* **2014**, *2* (13), 4682−4689.

(10) Yuan, Q.; Liu, D.; Zhang, N.; Ye, W.; Ju, H.; Shi, L.; Long, R.; Zhu, J.; Xiong, Y. Noble-Metal-Free Janus-Like Structures by Cation Exchange for Z-Scheme Photocatalytic Water Splitting under Broadband Light Irradiation. *Angew. Chem., Int. Ed.* **2017**, *56* (15), 4206−4210.

(11) Cho, G.; Kim, H.; Park, Y. S.; Hong, Y.-K.; Ha, D.-H. Phase Transformation of Iron Phosphide Nanoparticles for Hydrogen Evolution Reaction Electrocatalysis. *Int. J. Hydrogen Energy* **2018**, *43* (24), 11326−11334.

(12) Park, J.; Jin, H.; Lee, J.; Oh, A.; Kim, B.; Kim, J. H.; Baik, H.; Joo, S. H.; Lee, K. Highly Crystalline $Pd_{13}Cu_3S_7$ Nanoplates Prepared via Partial Cation Exchange of $Cu_{1.81}S$ Templates as an Efficient Electrocatalyst for the Hydrogen Evolution Reaction. *Chem. Mater.* **2018**, *30* (19), 6884−6892.

(13) Zhang, X. R.; Zhang, Y.; Chen, F. T.; Li, Y.; Zhang, S. S. Visual Detection of Single-Nucleotide Polymorphisms and DNA Methyltransferase Based on Cation-Exchange of CuS Nanoparticles and Click Chemistry of Functionalized Gold Nanoparticles. *Chem. Commun.* **2016**, *52* (90), 13261−13264.

(14) Song, W.; Zhang, N.; Luan, Z.; Zhang, X.; He, P. Application of a Cation-Exchange Reaction of CuS Nanoparticles and Fluorescent Copper Nanoparticles in a DNA Biosensor. *RSC Adv.* **2018**, *8* (27), 15248−15252.

(15) Jain, P. K.; Beberwyck, B. J.; Fong, L.-K.; Polking, M. J.; Alivisatos, A. P. Highly Luminescent Nanocrystals From Removal of Impurity Atoms Residual From Ion-Exchange Synthesis. *Angew. Chem., Int. Ed.* **2012**, *51* (10), 2387−2390.

(16) Hao, M.; Bai, Y.; Zeiske, S.; Ren, L.; Liu, J.; Yuan, Y.; Zarrabi, N.; Cheng, N.; Ghasemi, M.; Chen, P.; Lyu, M.; He, D.; Yun, J.-H.; Du, Y.; Wang, Y.; Ding, S.; Armin, A.; Meredith, P.; Liu, G.; Cheng, H.-M.; Wang, L. Ligand-Assisted Cation-Exchange Engineering for High-Efficiency Colloidal $Cs_{1-x}FA_xPbI_3$ Quantum Dot Solar Cells with Reduced Phase Segregation. *Nat. Energy* **2020**, *5* (1), 79−88.

(17) Wang, H.; Butler, D. J.; Straus, D. B.; Oh, N.; Wu, F.; Guo, J.; Xue, K.; Lee, J. D.; Murray, C. B.; Kagan, C. R. Air-Stable $CuInSe_2$ Nanocrystal Transistors and Circuits via Post-Deposition Cation Exchange. *ACS Nano* **2019**, *13* (2), 2324−2333.

(18) Lee, W. S.; Kang, Y. G.; Woo, H. K.; Ahn, J.; Kim, H.; Kim, D.; Jeon, S.; Han, M. J.; Choi, J.-H.; Oh, S. J. Designing High-Performance CdSe Nanocrystal Thin-Film Transistors Based on Solution Process of Simultaneous Ligand Exchange, Trap Passivation, and Doping. *Chem. Mater.* **2019**, *31* (22), 9389−9399.

(19) Fayette, M.; Robinson, R. D. Chemical Transformations of Nanomaterials for Energy Applications. *J. Mater. Chem. A* **2014**, *2* (17), 5965−5978.
(20) Yin, Y.; Rioux, R. M.; Erdonmez, C. K.; Hughes, S.; Somorjai, G. A.; Alivisatos, A. P. Formation of Hollow Nanocrystals Through the Nanoscale Kirkendall Effect. *Science* **2004**, *304* (5671), 711.
(21) Son, D. H.; Hughes, S. M.; Yin, Y.; Paul Alivisatos, A. Cation Exchange Reactions in Ionic Nanocrystals. *Science* **2004**, *306* (5698), 1009.
(22) Beberwyck, B. J.; Surendranath, Y.; Alivisatos, A. P. Cation Exchange: A Versatile Tool for Nanomaterials Synthesis. *J. Phys. Chem. C* **2013**, *117* (39), 19759−19770.
(23) Lokteva, I.; Radychev, N.; Witt, F.; Borchert, H.; Parisi, J.; Kolny-Olesiak, J. Surface Treatment of CdSe Nanoparticles for Application in Hybrid Solar Cells: The Effect of Multiple Ligand Exchange with Pyridine. *J. Phys. Chem. C* **2010**, *114* (29), 12784−12791.
(24) Lee, J.-S.; Kim, H.; Algar, W. R. Thiol-Ligand-Catalyzed Quenching and Etching in Mixtures of Colloidal Quantum Dots and Silver Nanoparticles. *J. Phys. Chem. C* **2017**, *121* (51), 28566−28575.
(25) Zhang, B.; Jung, Y.; Chung, H.-S.; Vugt, L. V.; Agarwal, R. Nanowire Transformation by Size-Dependent Cation Exchange Reactions. *Nano Lett.* **2010**, *10* (1), 149−155.
(26) Li, H.; Zanella, M.; Genovese, A.; Povia, M.; Falqui, A.; Giannini, C.; Manna, L. Sequential Cation Exchange in Nanocrystals: Preservation of Crystal Phase and Formation of Metastable Phases. *Nano Lett.* **2011**, *11* (11), 4964−4970.
(27) Fenton, J. L.; Steimle, B. C.; Schaak, R. E. Structure-Selective Synthesis of Wurtzite and Zincblende ZnS, CdS, and $CuInS_2$ Using Nanoparticle Cation Exchange Reactions. *Inorg. Chem.* **2019**, *58* (1), 672−678.
(28) Tan, J. M. R.; Scott, M. C.; Hao, W.; Baikie, T.; Nelson, C. T.; Pedireddy, S.; Tao, R.; Ling, X.; Magdassi, S.; White, T.; Li, S.; Minor, A. M.; Zheng, H.; Wong, L. H. Revealing Cation-Exchange-Induced Phase Transformations in Multielemental Chalcogenide Nanoparticles. *Chem. Mater.* **2017**, *29* (21), 9192−9199.
(29) Robinson, R. D.; Sadtler, B.; Demchenko, D. O.; Erdonmez, C. K.; Wang, L.-W.; Alivisatos, A. P. Spontaneous Superlattice Formation in Nanorods Through Partial Cation Exchange. *Science* **2007**, *317* (5836), 355.
(30) Lesnyak, V.; Brescia, R.; Messina, G. C.; Manna, L. Cu Vacancies Boost Cation Exchange Reactions in Copper Selenide Nanocrystals. *J. Am. Chem. Soc.* **2015**, *137* (29), 9315−9323.
(31) Wark, S. E.; Hsia, C.-H.; Son, D. H. Effects of Ion Solvation and Volume Change of Reaction on the Equilibrium and Morphology in Cation-Exchange Reaction of Nanocrystals. *J. Am. Chem. Soc.* **2008**, *130* (29), 9550−9555.
(32) Zhang, D.; Wong, A. B.; Yu, Y.; Brittman, S.; Sun, J.; Fu, A.; Beberwyck, B.; Alivisatos, A. P.; Yang, P. Phase-Selective Cation-Exchange Chemistry in Sulfide Nanowire Systems. *J. Am. Chem. Soc.* **2014**, *136* (50), 17430−17433.
(33) Imran, M.; Ijaz, P.; Goldoni, L.; Maggioni, D.; Petralanda, U.; Prato, M.; Almeida, G.; Infante, I.; Manna, L. Simultaneous Cationic and Anionic Ligand Exchange For Colloidally Stable $CsPbBr_3$ Nanocrystals. *ACS Energy Lett.* **2019**, *4* (4), 819−824.
(34) Beberwyck, B. J.; Alivisatos, A. P. Ion Exchange Synthesis of III−V Nanocrystals. *J. Am. Chem. Soc.* **2012**, *134* (49), 19977−19980.
(35) Powell, A. E.; Hodges, J. M.; Schaak, R. E. Preserving Both Anion and Cation Sublattice Features during a Nanocrystal Cation-Exchange Reaction: Synthesis of Metastable Wurtzite-Type CoS and MnS. *J. Am. Chem. Soc.* **2016**, *138* (2), 471−474.
(36) Anderson, B. D.; Tracy, J. B. Nanoparticle Conversion Chemistry: Kirkendall Effect, Galvanic Exchange, and Anion Exchange. *Nanoscale* **2014**, *6* (21), 12195−12216.
(37) Cho, G.; Park, Y.; Hong, Y.-K.; Ha, D.-H. Ion Exchange: an Advanced Synthetic Method for Complex Nanoparticles. *Nano Convergence* **2019**, *6* (1), 17.
(38) Shamsi, J.; Dang, Z.; Ijaz, P.; Abdelhady, A. L.; Bertoni, G.; Moreels, I.; Manna, L. Colloidal CsX (X = Cl, Br, I) Nanocrystals and Their Transformation to $CsPbX_3$ Nanocrystals by Cation Exchange. *Chem. Mater.* **2018**, *30* (1), 79−83.
(39) De Trizio, L.; Manna, L. Forging Colloidal Nanostructures via Cation Exchange Reactions. *Chem. Rev.* **2016**, *116* (18), 10852−10887.
(40) Ha, D.-H.; Moreau, L. M.; Honrao, S.; Hennig, R. G.; Robinson, R. D. The Oxidation of Cobalt Nanoparticles into Kirkendall-Hollowed CoO and Co_3O_4: The Diffusion Mechanisms and Atomic Structural Transformations. *J. Phys. Chem. C* **2013**, *117* (27), 14303−14312.
(41) Owen, J. Nanocrystal Structure. The Coordination Chemistry of Nanocrystal Surfaces. *Science* **2015**, *347* (6222), 615−6.
(42) Nevers, D. R.; Williamson, C. B.; Hanrath, T.; Robinson, R. D. Surface Chemistry of Cadmium Sulfide Magic-Sized Clusters: a Window into Ligand-Nanoparticle Interactions. *Chem. Commun.* **2017**, *53* (19), 2866−2869.
(43) Liu, Z.; Bekenstein, Y.; Ye, X.; Nguyen, S. C.; Swabeck, J.; Zhang, D.; Lee, S.-T.; Yang, P.; Ma, W.; Alivisatos, A. P. Ligand Mediated Transformation of Cesium Lead Bromide Perovskite Nanocrystals to Lead Depleted Cs_4PbBr_6 Nanocrystals. *J. Am. Chem. Soc.* **2017**, *139* (15), 5309−5312.
(44) Jin, R.; Zeng, C.; Zhou, M.; Chen, Y. Atomically Precise Colloidal Metal Nanoclusters and Nanoparticles: Fundamentals and Opportunities. *Chem. Rev.* **2016**, *116* (18), 10346−10413.
(45) Chen, Y.; Lai, Z.; Zhang, X.; Fan, Z.; He, Q.; Tan, C.; Zhang, H. Phase Engineering of Nanomaterials. *Nat. Rev. Chem.* **2020**, *4* (5), 243−256.
(46) Hodges, J. M.; Kletetschka, K.; Fenton, J. L.; Read, C. G.; Schaak, R. E. Sequential Anion and Cation Exchange Reactions for Complete Material Transformations of Nanoparticles with Morphological Retention. *Angew. Chem., Int. Ed.* **2015**, *54* (30), 8669−8672.
(47) Agarwal, R.; Krook, N. M.; Ren, M.-L.; Tan, L. Z.; Liu, W.; Rappe, A. M.; Agarwal, R. Anion Exchange in II−VI Semiconducting Nanostructures via Atomic Templating. *Nano Lett.* **2018**, *18* (3), 1620−1627.
(48) Yan, N.; Xia, N.; Wu, Z. Metal Nanoparticles Confronted with Foreign Ligands: Mere Ligand Exchange or Further Structural Transformation? *Small* **2020**, e2000609.
(49) Fenton, J. L.; Steimle, B. C.; Schaak, R. E. Tunable Intraparticle Frameworks for Creating Complex Heterostructured Nanoparticle Libraries. *Science* **2018**, *360* (6388), 513.
(50) Jain, P. K.; Amirav, L.; Aloni, S.; Alivisatos, A. P. Nanoheterostructure Cation Exchange: Anionic Framework Conservation. *J. Am. Chem. Soc.* **2010**, *132* (29), 9997−9999.
(51) Nelson, A.; Honrao, S.; Hennig, R. G.; Robinson, R. D. Nanocrystal Symmetry Breaking and Accelerated Solid-State Diffusion in the Lead−Cadmium Sulfide Cation Exchange System. *Chem. Mater.* **2019**, *31* (3), 991−1005.
(52) Dawood, F.; Schaak, R. E. ZnO-Templated Synthesis of Wurtzite-Type ZnS and ZnSe Nanoparticles. *J. Am. Chem. Soc.* **2009**, *131* (2), 424−425.
(53) Park, J.; Zheng, H.; Jun, Y.-w.; Alivisatos, A. P. Hetero-Epitaxial Anion Exchange Yields Single-Crystalline Hollow Nanoparticles. *J. Am. Chem. Soc.* **2009**, *131* (39), 13943−13945.
(54) Zhang, H.; Solomon, L. V.; Ha, D.-H.; Honrao, S.; Hennig, R. G.; Robinson, R. D. $(NH_4)_2S$, a Highly Reactive Molecular Precursor for Low Temperature Anion Exchange Reactions in Nanoparticles. *Dalton Trans.* **2013**, *42* (35), 12596−12599.
(55) Nelson, A.; Fritz, K. E.; Honrao, S.; Hennig, R. G.; Robinson, R. D.; Suntivich, J. Increased Activity in Hydrogen Evolution Electrocatalysis for Partial Anionic Substitution in Cobalt Oxysulfide Nanoparticles. *J. Mater. Chem. A* **2016**, *4* (8), 2842−2848.
(56) Dloczik, L.; Engelhardt, R.; Ernst, K.; Fiechter, S.; Sieber, I.; Könenkamp, R. Hexagonal nanotubes of ZnS by chemical conversion of monocrystalline ZnO columns. *Appl. Phys. Lett.* **2001**, *78* (23), 3687−3689.
(57) Jin fan, H.; Knez, M.; Scholz, R.; Nielsch, K.; Pippel, E.; Hesse, D.; Zacharias, M.; Gösele, U. Monocrystalline Spinel Nanotube

https://dx.doi.org/10.1021/acs.accounts.0c00704
Acc. Chem. Res. 2021, 54, 509−519

Fabrication based on the Kirkendall Effect. *Nat. Mater.* **2006**, *5* (8), 627−631.
(58) Yin, Y.; Alivisatos, A. P. Colloidal Nanocrystal Synthesis and the Organic−Inorganic Interface. *Nature* **2005**, *437* (7059), 664−670.
(59) White, S. L.; Banerjee, P.; Chakraborty, I.; Jain, P. K. Ion Exchange Transformation of Magic-Sized Clusters. *Chem. Mater.* **2016**, *28* (22), 8391−8398.
(60) Stein, J. L.; Steimle, M. I.; Terban, M. W.; Petrone, A.; Billinge, S. J. L.; Li, X.; Cossairt, B. M. Cation Exchange Induced Transformation of InP Magic-Sized Clusters. *Chem. Mater.* **2017**, *29* (18), 7984−7992.
(61) Li, Y.; Cheng, H.; Yao, T.; Sun, Z.; Yan, W.; Jiang, Y.; Xie, Y.; Sun, Y.; Huang, Y.; Liu, S.; Zhang, J.; Xie, Y.; Hu, T.; Yang, L.; Wu, Z.; Wei, S. Hexane-Driven Icosahedral to Cuboctahedral Structure Transformation of Gold Nanoclusters. *J. Am. Chem. Soc.* **2012**, *134* (43), 17997−18003.
(62) Kang, X.; Zhu, M. Transformation of Atomically Precise Nanoclusters by Ligand-Exchange. *Chem. Mater.* **2019**, *31* (24), 9939−9969.
(63) Lin, J.; Zhang, Q.; Wang, L.; Liu, X.; Yan, W.; Wu, T.; Bu, X.; Feng, P. Atomically Precise Doping of Monomanganese Ion into Coreless Supertetrahedral Chalcogenide Nanocluster Inducing Unusual Red Shift in Mn^{2+} Emission. *J. Am. Chem. Soc.* **2014**, *136* (12), 4769−4779.
(64) Wang, Y.; Liu, Y.-H.; Zhang, Y.; Wang, F.; Kowalski, P. J.; Rohrs, H. W.; Loomis, R. A.; Gross, M. L.; Buhro, W. E. Isolation of the Magic-Size CdSe Nanoclusters $[(CdSe)_{13}(n\text{-octylamine})_{13}]$ and $[(CdSe)_{13}(oleylamine)_{13}]$. *Angew. Chem., Int. Ed.* **2012**, *51* (25), 6154−6157.
(65) Yu, W. W.; Peng, X. Formation of High-Quality CdS and Other II−VI Semiconductor Nanocrystals in Noncoordinating Solvents: Tunable Reactivity of Monomers. *Angew. Chem., Int. Ed.* **2002**, *41* (13), 2368−2371.
(66) Vossmeyer, T.; Katsikas, L.; Giersig, M.; Popovic, I. G.; Diesner, K.; Chemseddine, A.; Eychmueller, A.; Weller, H. CdS Nanoclusters: Synthesis, Characterization, Size Dependent Oscillator Strength, Temperature Shift of the Excitonic Transition Energy, and Reversible Absorbance Shift. *J. Phys. Chem.* **1994**, *98* (31), 7665−7673.
(67) Wang, Y.; Zhou, Y.; Zhang, Y.; Buhro, W. E. Magic-Size II−VI Nanoclusters as Synthons for Flat Colloidal Nanocrystals. *Inorg. Chem.* **2015**, *54* (3), 1165−1177.
(68) Kudera, S.; Zanella, M.; Giannini, C.; Rizzo, A.; Li, Y.; Gigli, G.; Cingolani, R.; Ciccarella, G.; Spahl, W.; Parak, W. J.; Manna, L. Sequential Growth of Magic-Size CdSe Nanocrystals. *Adv. Mater.* **2007**, *19* (4), 548−552.
(69) Pan, D.; Ji, X.; An, L.; Lu, Y. Observation of Nucleation and Growth of CdS Nanocrystals in a Two-Phase System. *Chem. Mater.* **2008**, *20* (11), 3560−3566.
(70) Yu, Q.; Liu, C.-Y. Study of Magic-Size-Cluster Mediated Formation of CdS Nanocrystals: Properties of the Magic-Size Clusters and Mechanism Implication. *J. Phys. Chem. C* **2009**, *113* (29), 12766−12771.
(71) Nevers, D. R.; Williamson, C. B.; Savitzky, B. H.; Hadar, I.; Banin, U.; Kourkoutis, L. F.; Hanrath, T.; Robinson, R. D. Mesophase Formation Stabilizes High-Purity Magic-Sized Clusters. *J. Am. Chem. Soc.* **2018**, *140* (10), 3652−3662.
(72) Anderson, N. C.; Hendricks, M. P.; Choi, J. J.; Owen, J. S. Ligand Exchange and the Stoichiometry of Metal Chalcogenide Nanocrystals: Spectroscopic Observation of Facile Metal-Carboxylate Displacement and Binding. *J. Am. Chem. Soc.* **2013**, *135* (49), 18536−18548.

https://dx.doi.org/10.1021/acs.accounts.0c00704
Acc. Chem. Res. 2021, 54, 509−519